

# **Aerosol Science and Technology**



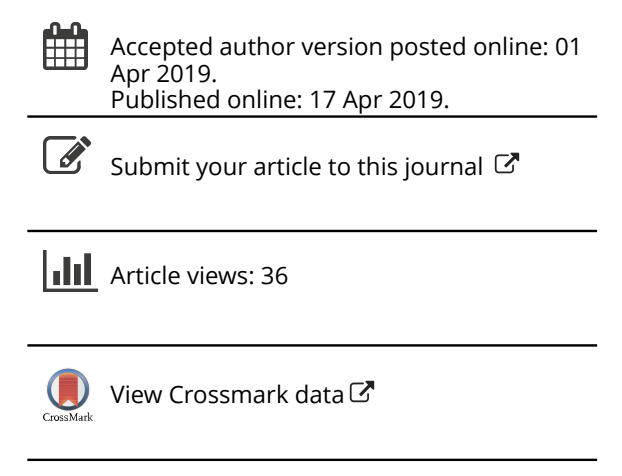
ISSN: 0278-6826 (Print) 1521-7388 (Online) Journal homepage: https://www.tandfonline.com/loi/uast20

# High resolution STEM/EDX spectral imaging to resolve metal distributions within ~100 nm combustion generated ash particles

Yueming Wang, Brian Van Devener, Xiaolong Li & Jost O. L. Wendt

To cite this article: Yueming Wang, Brian Van Devener, Xiaolong Li & Jost O. L. Wendt (2019): High resolution STEM/EDX spectral imaging to resolve metal distributions within ~100 nm combustion generated ash particles, Aerosol Science and Technology, DOI: 10.1080/02786826.2019.1601678

To link to this article: <a href="https://doi.org/10.1080/02786826.2019.1601678">https://doi.org/10.1080/02786826.2019.1601678</a>









# High resolution STEM/EDX spectral imaging to resolve metal distributions within $\sim$ 100 nm combustion generated ash particles

Yueming Wang<sup>a</sup> , Brian Van Devener<sup>b</sup>, Xiaolong Li<sup>a</sup>, and Jost O. L. Wendt<sup>a</sup>

<sup>a</sup>Department of Chemical Engineering and Institute for Clean and Secure Energy, University of Utah, Salt Lake City, Utah, USA; <sup>b</sup>Surface Analysis Laboratory, University of Utah, Salt Lake City, Utah, USA

#### **ABSTRACT**

Ultrafine ash particles play an important role in establishing a sticky inner deposit layer on heat transfer surface for power plants, but it is still unclear whether a thin surface alkali coating on these ultrafine particles might control this deposition behavior. In this research, we used a high resolution FE-TEM/STEM equipped with twin SDD EDX detectors for high X-ray detection efficiency, to determine the presence and absence of surface enrichment of alkali metals on ultrafine solid fuel ash samples that had low bulk alkali compositions but high deposition rates. Results from two types of combustion generated nano-sized ash particles are presented. One was from the oxy-combustion of pulverized bituminous coal, the other from oxy-combustion of pulverized rice husks, both being burned in a 100 kW rated down-flow laboratory combustor. Elemental mapping results from STEM/EDX uncovered some surface enrichment of alkali metals in ultrafine ash particles, where it existed, as it did for combustion of rice husks. However, it was not able to discern similar alkali metal surface enrichment for the bituminous coal ultrafines that had resulted in even higher deposition rates. Since deposition rates from both of these cases lie on the same correlation with PM<sub>1</sub>, one can conclude that although surface enrichment of alkali metals is present for some  $\sim$ 100 nm particles, it is not a prerequisite to achieve high inner surface deposition rates. This is in contrast to prevailing theories that point to alkali metals as "bad actors" as far as the sticky inner deposition rate is concerned.

#### **ARTICLE HISTORY**

Received 7 December 2018 Accepted 22 March 2019

**EDITOR** Matti Maricq

#### 1. Introduction

The generation of inorganic ultrafine/nanoparticles during coal/biomass combustion process is one of the major issues for power plants. First, the ultrafine fly ash particles can deposit on heat transfer surface and stimulate the formation of ash deposition (Li et al. 2015; Zhan and Wendt 2017), which can significantly decrease the heat transfer efficiency and even cause costly boiler shutdown (Bryers 1996). Second, the entrained ultrafine particulates in the flue gas cannot be efficiently captured by pollution control devices and can make a significant contribution to ambient airborne particulate matter (PM). These released ultrafine particles have very long atmospheric residence times and could thus cause serious environmental and human health risk (Donaldson et al. 2005; Lighty, Veranth, and Sarofim 2000). Numerous studies have been conducted to determine the existence of hazardous elements (As, Cd, Pb, Hg, Sn, etc.) in ultrafine/

nanoparticles and some of these studies can be found in a recent review paper (Saikia et al. 2018). In general, most reported studies on combustion generated ultrafine particles are concerned with the health effects and little is available about their effect on ash deposition formation. Therefore, the objective of this work is to shed light on the understanding of the effects of ultrafine aerosols on ash deposition formation.

Among the very few available literature references concerned with the relationship between ultrafine particles and ash deposition, Li et al. (2015) reported that the ultrafine particles generated from Zhundong lignite are mostly composed of sodium sulfate and sodium chloride, that these particles can deposit on heat transfer surface by thermophoresis force and subsequently form the sticky inner layer. This sticky inner layer can thus capture additional large particles on the wall, which can be denoted as a "glue effect." Zhan and Wendt also discovered the "glue effect." of ultrafine particles and their studies suggested that ultrafine

particles do not necessarily consist of measurable bulk amounts of alkali metal rich minerals (Zhan and Wendt 2017). They further suggested that the growth rates of sticky inner deposits depend on the concentration of submicron particles in the flue gas regardless of their composition. However, the compositions of ultrafine particles in Zhan and Wendt's work were measured by scanning electron microscopy (SEM) with energy dispersive X-ray spectroscopy (EDX), which can only provide the bulk composition of ultrafine particles. Hence, it is still unclear whether there exists a surface coating of alkali metals in ultrafine particles. A small amount of alkali rich minerals (such as Na<sub>2</sub>SO<sub>4</sub>, NaCl) on the surface might not significantly change the particle's bulk composition, but it can greatly decrease the viscosity of surface material that can cause the particle to stick. Therefore, to understand the role of alkali metals, it is important to understand the distribution of alkali metals within the ultrafine particles, not just their bulk concentrations.

Particles with diameter smaller than 100 nm are referred as ultrafine particles in this article. During the combustion process, a few percent of inorganic minerals can be vaporized and converted into inorganic vapors. Volatile elements such as Na, K, Cl, P, and S are more readily vaporized than refractory elements, but a small portion of refractory metal oxide ash (SiO<sub>2</sub>, CaO, and MgO) can be reduced by CO during char oxidation process to form volatile inorganic vapors (SiO, Ca, and Mg) (Quann and Sarofim 1982). After being released from the char particles, these inorganic vapors nucleate to form nano-sized nuclei, which can further grow in size through coagulation and generate ultrafine particles (Xu et al. 2011). These processes are greatly affected by the fuel properties and combustion conditions (Liu, Wang, and Wendt 2017). Due to the small size and high surface area, ultrafine particles have a greater tendency to absorb hazardous elements that are transferred from coal ash to vapor phase during combustion process (Saikia et al. 2015).

The morphology, size, and composition of micron and even submicron fly-ash particles have been well characterized by a variety of techniques (Vassilev and Vassileva 2005). Although the average bulk compositional information of a group of ultrafine particles can be analyzed by SEM/EDX, the individual ultrafine particle itself cannot be characterized by this technique. Nevertheless, a multiparametric characterization of size, chemical composition, and atomic structure of individual ultrafine particles can be analyzed by high resolution transmission electron

microscopy (HR-TEM). HR-TEM usually has a high spatial resolution at the atomic scale, and it can provide direct images and compositional information of individual nanoparticles at a spatial resolution down to atomic dimensions (<1 nm) when it is coupled with EDX. Satoshi Utsunomiya, Rodney Ewing, and their research groups have published numerous studies concerning the characterization of ultrafine airthe environment. They particulates in determined the existence of heavy metals (Pb, As, La, Ce, Sr, Zn, Cr, Se, Sn, Y, Zr, Au, and Ag) in ultrafine atmospheric aerosols through high-angle annular dark field scanning TEM (HAADF-STEM) and energy-filtered TEM (EFTEM) (Utsunomiya and Ewing 2003; Utsunomiya et al. 2004). Using these techniques, they were able to identify the nanocrystals of uraninite  $(UO_{2+x})$  in carbonaceous matter ( $\leq 50 \text{ nm}$ ) for the first time (Utsunomiya et al. 2002). More importantly, they further utilized the electron tomography to obtain the three-dimensional structure of samples at nanometer scale (Utsunomiya et al. 2011). HAADF-STEM is also utilized in this article to characterize the metal distributions of individual ultrafine particles.

The work described in this article builds on the pioneering work of Chen et al., who were among the first to investigate the properties of ultrafine coal fly ash using transmission electron microscopy (Chen et al. 2005a, 2005b). They showed that ultrafine coal fly ash could have quite different morphologies, compositions, and microstructures compared with supermicron coal fly ash, but did not focus specifically on surface enrichment in alkali metals, and did not relate their results to deposition behavior. The ultrafine combustion generated particles could consist of various minerals such as nano-sized aluminosilicate glass, ferrian spinel, hematite, magnetite, mullite, and quartz, depending on the fuel properties and combustion condition (Ribeiro et al. 2013; Silva and da Boit 2011). For example, the ultrafine aerosols from Western Kentucky coal are mainly composed of Al-Ti rich minerals, while the major chemical categories for ultrafine aerosols from Wyoming PRB coal are Ca-P rich minerals (Chen et al. 2005c). Typically, ultrafine coal fly ash particles are composed of a large amount of alkali and alkaline earth metals (AAEM) (Xu et al. 2016), and the yield of AAEM in ultrafine particles would be reduced if aluminum-silicon content is increased in the fuel (Ruan et al. 2018). However, little is known for the characteristics of ultrafine fly ash from biomass combustion. In order to fill this gap, the ultrafine fly ash from coal and biomass combustion will be both investigated in this article.

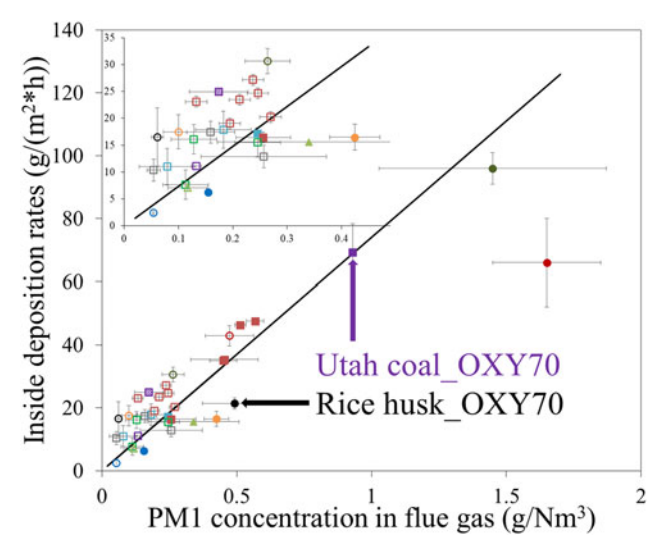


Figure 1. Inside deposition rates correlation with PM<sub>1</sub> concentration in flue gas (Wang, Li, and Wendt 2019).

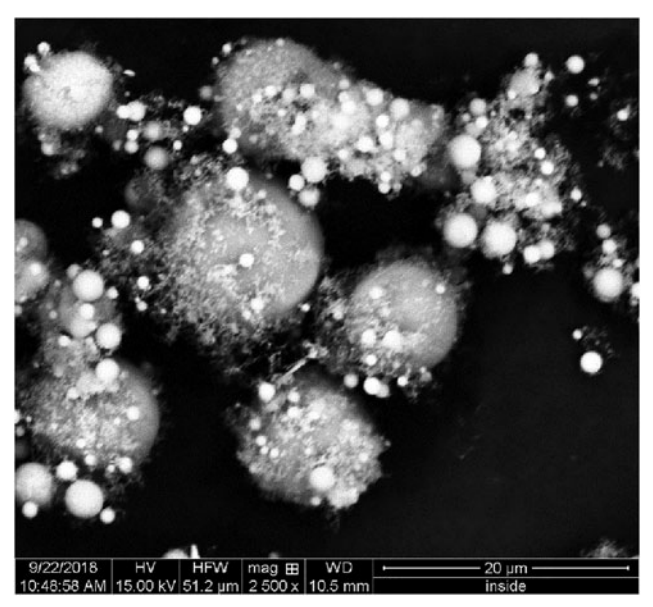


Figure 2. SEM images of inner deposits of Utah coal under oxy-combustion (Wang, Li, and Wendt 2019).

#### 2. Methods

## 2.1. Generation of ultrafine fly ash particles

All the ultrafine fly ash particles investigated in this work were generated in a 100 kW (rated) down-fired oxy-fuel combustor (OFC) at University of Utah's industrial combustion and gasification research facility (ICGRF). OFC is a self-sustained pilot-scale reactor and it mainly consists of an ignition zone, a radiation zone, and a convection zone. OFC can be systematically controlled, and it operates at realistic stoichiometric ratios, with turbulent diffusion flames in ignition

zone causing realistic temperature/time profiles, which are comparable to practical units. The ash aerosols are sampled downstream where the exhaust gases become laminar. The OFC has been extensively used in previous studies for various pulverized solid fuels including coal and biomass, and details regarding its configuration can be found elsewhere (Wang, Li, and Wendt 2018; Zhan et al. 2016; Zhang et al. 2011; Zhou et al. 2019).

Size classified ash aerosols were sampled by an isokinetic, water-cooled sampling probe. The sampled aerosol was quenched by the nitrogen at the inlet to avoid the further coagulation and water condensation inside the probe. The particle size distributions (PSDs) of the sampled ash aerosols were obtained using online electric mobility technique (SMPS: 0.0143-0.672 µm) and light scattering technique (APS: 0.532-20 µm) combo. The size segregated ash aerosols were collected by an 11-stage Berner low pressure impactor (BLPI: 0.0324-15.7 µm), which is based on particle aerodynamic behavior. Although different physical principles are the behind the operation of these three instruments for PSD measurements, the resulting PSDs from SMPS/APS match well with that from BLPI for the investigated cases in this article. More details concerning aerosol analysis technique can be found elsewhere (Wang, Li, and Wendt 2018). The aerosol samples with cutoff size of 0.168 µm are selected to represent ultrafine particles in this work.

The ash deposit is collected by a temperature controlled probe, which has been described in details by Zhan et al. (2013). The wall temperature on the probe is controlled through the adjustable air flow and inserted thermocouple. The deposit probe is inserted in post-flame zone to collect fouling ash deposition that are formed in laminar convection zone by inertial impaction and thermophoresis force. Typically, the skin temperature of the probe is controlled at 922 K and the surrounding flue gas temperature is about 1300 K. The collected ash deposits on horizontal surface of the probe can be mainly divided into tightly bound sticky inner deposits and loosely bound outer deposits. As described above, the "glue effect" of ultrafine particles can promote the formation of sticky inner deposits, thus only inner deposits will be involved in the article.

# 2.2. The "glue effect" of ultrafine fly ash particles

The characteristics of ash aerosols from different solid fuels with various combustion conditions have been analyzed and reported elsewhere (Wang, Li, and Wendt 2019), and the relationship between inner deposits growth rates (or inside deposition rates) and submicron particle concentrations is recapped and shown in Figure 1. It clearly suggests that higher PM<sub>1</sub> concentration corresponds to higher inside deposition rate, and this is explained as the "glue effect" of submicron particles. Figure 2 shows the SEM image of inner deposits from Utah coal oxy-combustion, which suggests that submicron/ ultrafine particles indeed have the "glue effect" and tend to stick on the surface of large particles (Wang, Li, and Wendt 2019). As mentioned above, the "glue effect" of submicron particles has not been well understood yet, the possibility of surface coating of alkali contents need to be further determined. For this purpose, the sampled ash aerosols from rice husk and Utah Sufco coal #2 (denoted as Utah coal afterwards) will be further studied to determine the metal distributions in ultrafine aerosols that are generated from biomass and coal combustion. Both fuels were burned under oxy-combustion with oxygen concentration of 70% (denoted as OXY70). More details about the combustion conditions of these two cases can be found elsewhere (Liu, Wang, and Wendt 2017; Wang, Li, and Wendt 2018). As shown in Figure 1, both selected cases have high inside deposition rates along with high concentration.

#### 3. Results and discussion

# 3.1. Ultrafine fly ash particles from rice husk oxy-combustion

The bulk compositions of raw rice husk ash and ultrafine fly ash from oxy-combustion are measured by SEM/EDX and the results are presented in column I and II of Figure 3. An FEI Quanta 600 FEG SEM operated at 15 kV, coupled with an EDAX<sup>TM</sup> EDX system with a Si(Li) X-ray detector was used for the SEM/EDX measurements. Quantitative analysis of SEM/EDX results was obtained using the standardless, matrix effect ZAF correction method (where Z is the atomic number correction, A is the absorption correction, and F is the secondary fluorescence correction) built into the EDAX<sup>TM</sup> Genesis software that was also used to collect the data. Any results obtained from standardless EDX quantification routines must be treated with caution as they are commonly misinterpreted. As noted by Newbury (1998), results from standardless quantification as applied to non-homogenous, topographically rough samples which are

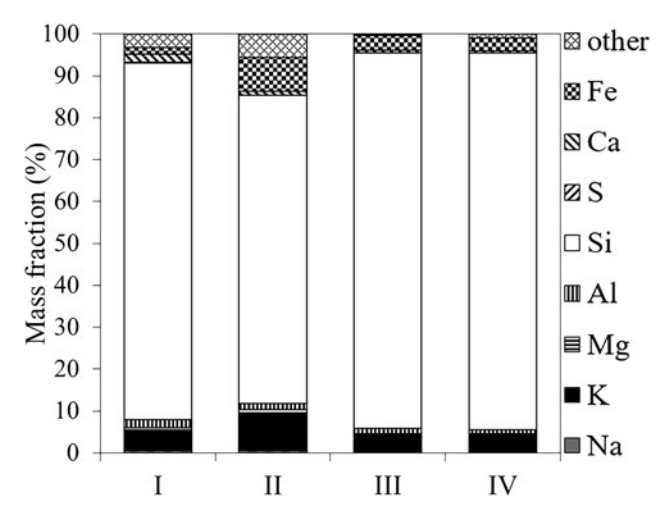


**Figure 3.** C and O free compositions measured by EDX ("other" represents the sum of P, Cl, Mn, and Ti): (I) raw rice husk ash composition; (II) bulk composition of ultrafine fly ash; (III) composition of individual particles from Figure 4(a); (IV) composition of individual particles from Figure 4(b).

comprised of major and minor constituents (such as is the case with these samples), must be viewed in terms of relative rather than absolute amounts. Thus, the reported compositional results must be interpreted cautiously, and the "quantitative" bulk composition analysis herein should only be used for comparison purposes. As EDS provides data of high precision (although not necessarily of high accuracy), and these samples have similar topography and major/minor elemental constituents, the inter-sample comparison of wt.% is still valid.

As shown in Figure 3, there are appreciable amounts (9.6%) of alkali metals (Na and K) in bulk ultrafine fly ash, and the concentrations of potassium and sodium in ultrafine fly ash are separately 100.2% and 5.5% higher than that in raw ash. Moreover, the iron in ultrafine fly ash is even 410.1% higher than that in raw ash. Despite the enrichment of alkali metals and iron in ultrafine fly ash, the majority (73.4%) of the ultrafine fly ash is composed of Si. This finding for ultrafine particles in rice husk combustion is different from the research by Han et al. (2019), where they indicated that ultrafine particles are dominated by K, Cl, and P. This controversy might be caused by: (1) the higher peak gas temperature in this study (1705 K) than that in Han's (1575 K), which causes stronger vaporization of silica in this study; (2) the lower K<sub>2</sub>O in rice husk ash in this study (2.66%) than that in Han's (5.78%). Although the bulk composition of ultrafine fly ash is dominated by Si, the possible surface coating of alkali rich minerals could significantly reduce the

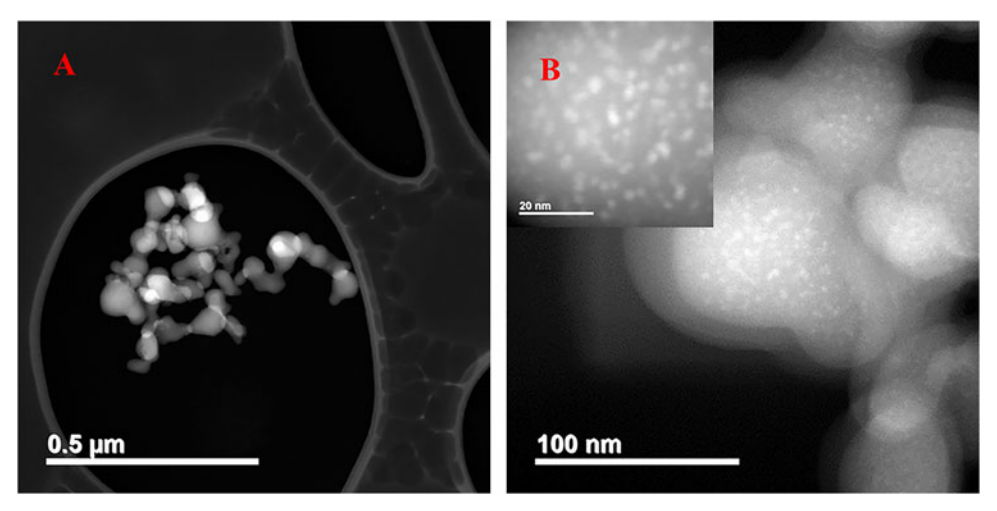


Figure 4. HAADF images of ultrafine particles from rice husk oxy-combustion.

particle viscosity at the surface and increase the sticking probability. Therefore, it is important to determine whether silicon and alkali metals are homogeneously distributed inside the ultrafine particulates or the alkali metals are adhered on the surface of pure silica nucleus.

STEM/EDX was utilized to analyze individual ultrafine fly ash particles. During sample preparation, 1 mg of particles are dispersed in 10 mL ethanol by sonication for 1 h. Afterwards, a 5 µL solution droplet is applied to the TEM grid (ultrathin carbon film supported by a lacey carbon film on a 400 mesh copper grid from Ted Pella, Product No. 01824), and the aerosol samples are mounted to the grid after drying for 20 min. A 200 kV JEOL 2800 STEM with dual SDD EDX detectors was used to collect the data. HAADF images, which were collected with a detector semi angle of 62.1 mrad, are shown in Figure 4. Figure 4a shows the cluster of a number of ∼100 nm primary particles, Figure 4b shows the partially enlarged image of primary particles. With the high resolution of the STEM, the insert in Figure 4b indicates that there exist some nanoparticles (~2 nm) on the surface of the ultrafine particles. As brighter regions in HAADF images correlate to sample regions that have higher atomic density, so called "z" contrast, these bright nanoparticles must be rich in a relatively heavier element. This will be discussed in more detail later. These ultrafine fly ash formed though the vaporization and nucleation should be in spherical shape, but the ∼100 nm primary particles have some extent of deformation and are sintered together to form the cluster (indicated by the arrow in Figure 4b). The reason for the sintering will be discussed in more details below.

Figure 5 presents the elemental mapping for the particles that are investigated in Figure 4. The reduced X-ray analytical volume in STEM/EDX, necessary high probe currents, and instrument design limitations have typically limited this kind of analysis as applied to beam sensitive samples such as combustion generated ash. The dual SDD EDX detector system on the JEOL 2800 at Utah, with a combined detector area of 200 mm<sup>2</sup> and nominal solid angle of detection of 1.9 sr helps to overcome these traditional limitations. For elemental mapping data acquisition, the spectral images are processed using the ThermoScientific NSS software. The spectral images are background subtracted using "net counts" and a  $5 \times 5$  "Kernel Size," high "Quant Map Detail" and high precision of "Filter Fit Type" are applied using the software. Here, we only show spectral images for the most abundant elements measured (C, O, Al, Si, K, Ca, and Fe). Note that trace amounts of elements such as Na and S were also detected in the EDX spectra, but are not shown in the spectral images for clarity. The correction method of "Cliff-Lorimer" (Cliff and Lorimer 1975) was utilized for the quantitative analysis in STEM/ EDX. As was the case for the SEM/EDX results discussed earlier, these standardless quantification results must be interpreted in relative rather than absolute terms. The resultant concentrations are presented in column III and IV of Figure 3.

It should be noticed that there exists considerable difference in composition between bulk ultrafine particles (column II) and individual ultrafine particles (columns III and IV), which might be caused by the singularity of the investigated individual particles. Overall, it suggests that Si is the dominating element, and there are only small amounts of Al, K, Ca, and Fe

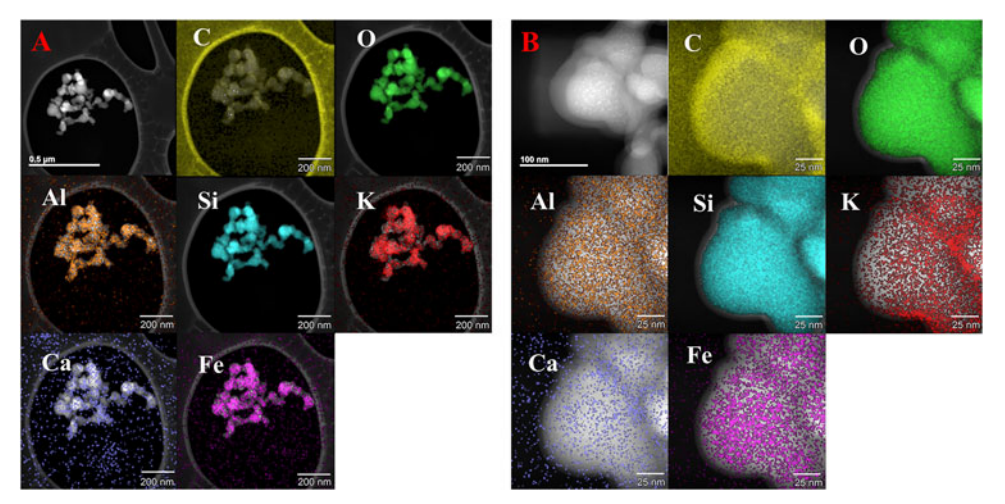
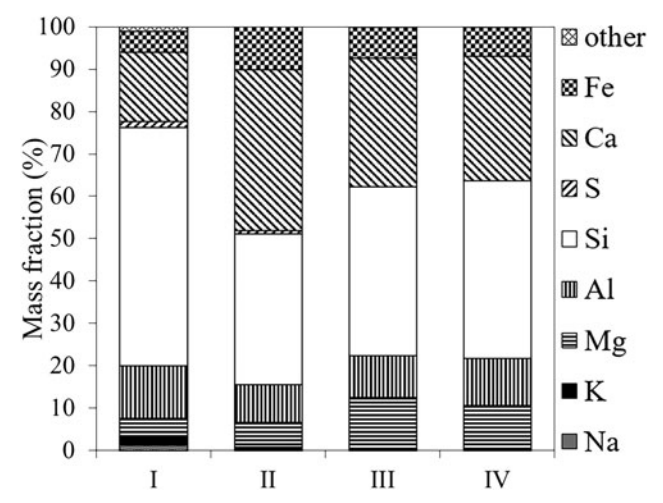


Figure 5. Elemental mapping results from STEM/EDX for the distribution of C, O, Al, Si, K, Ca, and Fe in individual particles.

sparsely distributed within the particles. With a lower magnification in Figure 5a, the ultrafine primary particles do not show significant compositional difference. With a higher magnification in Figure 5b, it is indicated that potassium is more enriched on the surface of primary particles especially in the place where primary particles are jointed. This enrichment indicates that the sintering of primary particles might be caused by the thin film of potassium associated minerals on the surface, which is formed through the condensation of potassium rich fumes. The thickness of this thin film is less than 10 nm and cannot be recognized by bulk composition analysis, thus it is important to obtain high resolution elemental mapping in order to resolve the metal distributions.

As mentioned earlier, the nanoparticles adhered on the surface are rich in an element of higher atomic number (see Figure 4b). Correlation to the EDX results, which show the heaviest element detected as Fe, it is reasonable to assume that these nanoparticles are composed of iron rich minerals, likely iron oxide. The iron contents in rice husk might be mainly associated with organic matrix, which could generate nanosized iron oxides during oxidative decomposition. These nano-sized iron oxides can be further interact with silicate, thus surface enrichment of nano-sized iron oxides are detected on silicate rich particles. Furthermore, carbon is also enriched on the surface of ultrafine particulates as shown in Figure 5b, which might be primary soot particles. It is not unusual to have carbon contents on the surface of ultrafine fly ash particles (Linak et al. 2007). It should be noted that the distribution of Ca is a little vague, because it is hard to get enough signal to determine its spatial distribution with a low concentration in rice husk ash (1.31%).



**Figure 6.** C and O free basis compositions ("other" represents the sum of P, Cl, Mn, and Ti) measured by EDX: (I) raw Utah coal ash composition; (II) bulk composition of ultrafine fly ash; (III) composition of individual particles from Figure 7(a); (IV) composition of individual particles from Figure 7(b).

# 3.2. Ultrafine fly ash particles from bituminous coal oxy-combustion

The ultrafine fly ash generated from the oxy-combustion of Utah coal is also investigated, and the bulk compositions of raw Utah coal ash and ultrafine fly ash were measured by SEM/EDX and the results can be found in columns I and II of Figure 6. For ultrafine fly ash, the concentrations of potassium and sodium are 68.5% and 81.2% lower than, while the iron is 106.2% higher than that in raw Utah coal ash. The results for alkali metals are contrary to the findings in rice husk oxy-combustion, which might be caused by more intense scavenging effect of alumniosilicates in Utah coal oxy-combustion. It was demonstrated that partitioning of alkali metals in the vapor and the subsequent fraction in the formed ultrafine

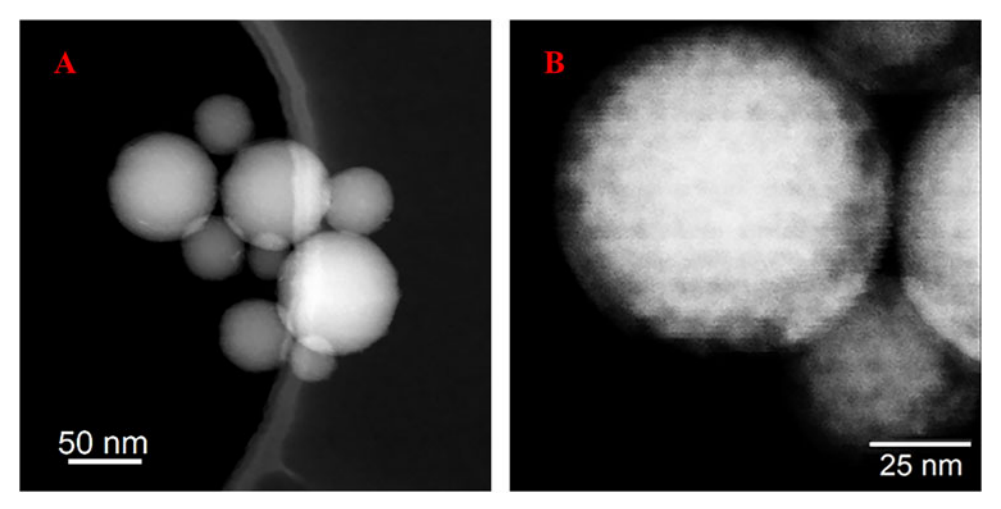


Figure 7. HAADF images of ultrafine particles from Utah coal oxy-combustion.

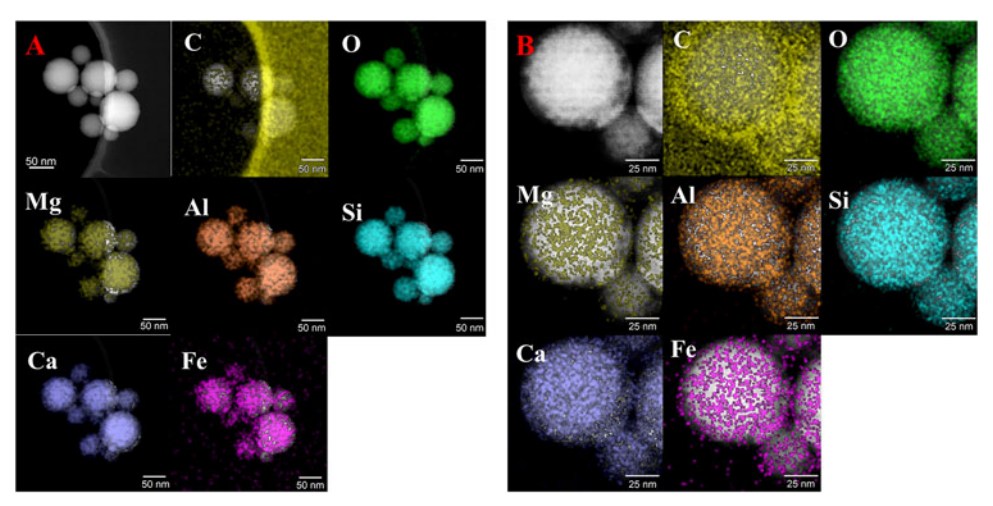


Figure 8. Elemental mapping results from STEM/EDX for the distribution of O, Mg, Al, Si, Ca, and Fe in individual particles.

aerosol can be greatly reduced by the presence of alumniosilicates under high temperature (Gallagher, Peterson, and Wendt 1996; Zhan et al. 2015). This scavenging effect on alkali metals is more intense in Utah coal oxy-combustion than that in rice husk oxycombustion because: (1) silica contents are abundant in both fuels, but the alumina content in Utah coal ash (12.9%) is much more than that in rice husk ash (1.73%), causing more alumniosilicates in Utah coal during combustion process; (2) the peak gas temperature is higher in Utah coal oxy-combustion ( $\sim$ 1866 K) than that in rice husk oxy-combustion ( $\sim$ 1705 K), causing higher reaction rates. Therefore, there are less alkali metals retained in the fume for Utah coal oxycombustion, which further causes lower concentration of alkali metals in the formed ultrafine particles. Moreover, Ca is 131.2% more enriched in ultrafine aerosols. The high concentration of Mg, Al, Si, and Ca suggest that Ca-Mg aluminosilicates is the major constituent for ultrafine fly ash.

Figure 7 presents the HAADF images of some ultrafine particles from Utah coal oxy-combustion. These ultrafine fly ash particles have good spherical shape. It has been reported that the formation of ultrafine particles in coal combustion primarily occurs near the solid fuel particles within the surrounding boundary layer (Liu, Wang, and Wendt 2017). There exists extreme high temperature and reducing environment near the burning fuel particles, thus the ultrafine particles can consist of significant amount of refractory elements such as Mg, Al, and Si as mentioned above. The ultrafine particles also tend to agglomerate together as shown in both Figures 7a and b. It should be noted that these particles showed more beam sensitivity than the rice husk generated ultrafine particles. This required imaging with lower probe current (nominally 59 pA) and shorter scanning time per pixel. Thus, the HAADF image shown in Figure 7b is noisier due to reduced image contrast and no nanoparticles can be distinguished here. However, for EDX

we were still able to obtain reasonable net counts of characteristic X-rays for detected elements to collect spectral image maps.

In order to determine the relative composition of these ultrafine particles, the elemental mapping for Figures 7a and b was conducted and the results are presented in Figures 8a and b separately. The same data acquisition process from Figure 5 is applied for Figure 8. Once again, only the abundant elements are investigated and reported (C, O, Mg, Al, Si, Ca, and Fe). The quantitative analysis of Figures 8a and b is presented in columns III and IV of Figure 6 through same methodology as mentioned above. Overall, there are considerable amounts of Si, Mg, Al, Ca, and Fe in ultrafine fly ash particles. There are no alkali metals detected in the investigated individual particles, which is consistent with the extreme low concentration of alkali metals in bulk composition as shown in column II of Figure 6. Similar with Figure 5b, carbon also tends to be enriched on the surface for Utah coal ultrafine particle as shown in Figure 8b. Although the concentration of alkali metals is extremely low in both bulk composition and surface of ultrafine particles, these particles still tend to adhere on large particles and promote the formation of inner deposits as shown in Figures 1 and 2. Therefore, the "glue effect" of ultrafine particles are not necessarily caused by the presence of alkali metals in either the bulk or on the surface the particles.

## 4. Conclusions

Ultrafine fly ash particles generated from oxy-combustion of Utah coal and rice husks were investigated in this work to study their "glue effect" necessary to form sticky inner ash deposits on heat transfer surfaces. The bulk compositions of raw fuel ash and generated ultrafine particles were obtained through SEM/ EDX, while the composition and elemental mapping of individual ultrafine fly ash particles were obtained through high resolution STEM/EDX.

With dual EDX detectors in the system, the collection time can be significantly reduced and the sample drifting can be minimized, thus allowing the measurement accuracy to be improved. The comparison between rice husk results and Utah coal results suggest that the physicochemical properties of ultrafine particles highly depend on the raw ash composition and the peak gas temperature. More aluminosilicates in raw ash and higher peak gas temperature can scavenge more alkali metals from the fume and cause less concentration of alkali metals in the formed ultrafine particles. These ultrafine particles can consist of a significant amount of refractory elements such as silica and Ca-Mg aluminosilicates under high temperature oxy-combustion. The surface of the ultrafine particles from rice husk contain iron rich nanoparticles, being generated from the organically associated iron contents. The surface coating of alkali metals in ultrafine particles is found for rice husk oxy-combustion but not for Utah coal oxy-combustion. Furthermore, the concentration of alkali metals in ultrafine particles bulk composition is extremely low for Utah coal oxycombustion, but the sticky inner deposition rates are very high. This suggests formation mechanisms for the strong inner deposits do not depend on the concentration of alkali metals either in the bulk or on the surface of ultrafine particles. The deposit depends primarily on the concentration of ultrafine particles of any composition, in the flue gas. In addition these findings suggest that the unique technique of high resolution STEM with dual EDX detectors is a powerful tool to resolve the elemental distribution within ultrafine fly ash particles.

# **Funding**

The authors would like to acknowledge financial support from the National Science Foundation through Award 1603249. This work also made use of University of Utah shared facilities of the Micron Technology Foundation Inc. Microscopy Suite sponsored by the College of Engineering, Health Sciences Center, Office of the Vice President for Research, and the Utah Science Technology and Research (USTAR) initiative of the State of Utah. This work also made use of University of Utah USTAR shared facilities supported, in part, by the MRSEC Program of the NSF Award 1121252.

# **ORCID**

Yueming Wang http://orcid.org/0000-0002-2059-4315

### References

Bryers, R. W. 1996. Fireside slagging, fouling, and high-temperature corrosion of heat-transfer surface due to impurities in steam-raising fuels. Prog. Energy Combust. Sci. 22 (1):29-120. doi:10.1016/0360-1285(95)00012-7.

Chen, Y., N. Shah, F. Huggins, G. Huffman, and A. Dozier. 2005a. Characterization of ultrafine coal fly ash particles by energy-filtered TEM. J. Microsc. 217 (Pt 3):225-234. doi:10.1111/j.1365-2818.2005.01445.x.

Chen, Y., N. Shah, F. E. Huggins, and G. P. Huffman. 2005b. Characterisation of fine and ultrafine fly ash by electron microscopy techniques. World of Coal Ash (WOCA), April 11-15, Lexington, Kentucky, USA.

- Chen, Y., N. Shah, F. E. Huggins, and G. P. Huffman. 2005c. Transmission electron microscopy investigation of ultrafine coal fly ash particles. Environ. Sci. Technol. 39: 1144-1151. doi:10.1021/es049871p.
- Cliff, G., and G. W. Lorimer. 1975. The quantitative analysis of thin specimens. J. Microsc. 103 (2):203-207. doi: 10.1111/j.1365-2818.1975.tb03895.x.
- Donaldson, K., L. Tran, L. A. Jimenez, R. Duffin, D. E. Newby, N. Mills, W. MacNee, and V. Stone. 2005. Combustion-derived nanoparticles: A review of their toxicology following inhalation exposure. Part. Fibre Toxicol. 2 (1):10. doi:10.1186/1743-8977-2-10.
- Gallagher, N. B., T. W. Peterson, and J. O. L. Wendt. 1996. Sodium partitioning in a pulverzed coal combustion environment. Symp. (Int.) Combust. 26 (2):3197-3204. doi:10.1016/S0082-0784(96)80165-2.
- Han, J., D. Yu, X. Yu, F. Liu, J. Wu, X. Zeng, G. Yu, and M. Xu. 2019. Effect of the torrefaction on the emission of PM10 from combustion of rice husk and its blends with a lignite. Proc. Combust. Inst. 37 (3):2733-2740. doi: 10.1016/j.proci.2018.07.011.
- Li, G., S. Li, Q. Huang, and Q. Yao. 2015. Fine particulate formation and ash deposition during pulverized coal combustion of high-sodium lignite in a down-fired furnace. Fuel 143:430-437. doi:10.1016/j.fuel.2014.11.067.
- Lighty, J. S., J. M. Veranth, and A. F. Sarofim. 2000. Combustion aerosols: Factors governing their size and composition and implications to human health. J. Air Waste Manage. Assoc. 50:1565-1618. doi:10.1080/ 10473289.2000.10464197.
- Linak, W. P., J.-I. Yoo, S. J. Wasson, W. Zhu, J. O. Wendt, F. E. Huggins, Y. Chen, N. Shah, G. P. Huffman, and M. I. Gilmour. 2007. Ultrafine ash aerosols from coal combustion: characterization and health effects. Proc. Combust. Inst. 31 (2):1929–1937. doi:10.1016/ j.proci.2006.08.086.
- Liu, H., Y. Wang, and J. O. L. Wendt. 2017. Particle size distributions of fly ash arising from vaporized components of coal combustion - A comparison of theory and experiment. Energy Fuels 32:4300-4307. doi:10.1021/ acs.energyfuels.7b03126.
- Newbury, D. E. 1998. Standardless quantitative electronexcited X-ray microanalysis by energy-dispersive spectrometry: what is its proper role? Microsc. Microanal. 4 (06):585-597. doi:10.1017/\$1431927698980564.
- Quann, R., and A. Sarofim. 1982. Vaporization of refractory oxides during pulverized coal combustion. Symp. (Int.) Combust. 19 (1):1429-1440.doi:10.1016/S0082-0784(82)80320-2.
- Ribeiro, J., K. DaBoit, D. Flores, M. A. Kronbauer, and L. F. Silva. 2013. Extensive FE-SEM/EDS, HR-TEM/EDS and ToF-SIMS studies of micron-to nano-particles in anthracite fly ash. Sci. Total Environ. 452:98-107. doi:10.1016/ j.scitotenv.2013.02.010.
- Ruan, R., H. Tan, X. Wang, Y. Li, S Li, Z. Hu, B. Wei, and T. Yang. 2018. Characteristics of fine particulate matter formation during combustion of lignite riched in AAEM (alkali and alkaline earth metals) and sulfur. Fuel 211: 206-213.
- Saikia, B. K., J. Saikia, S. Rabha, L. F. Silva, and R. Finkelman. 2018. Ambient nanoparticles/nanominerals and hazardous elements from coal combustion activity:

- implications on energy challenges and health hazards. Geosci. Front. 9 (3):863–875. doi:10.1016/j.gsf.2017.11.013.
- Saikia, B. K., C. R. Ward, M. L. Oliveira, J. C. Hower, F. De Leao, M. N. Johnston, A. O'Bryan, A. Sharma, B. P. Baruah, and L. F. Silva. 2015. Geochemistry and nanomineralogy of feed coals, mine overburden, and coalderived fly ashes from Assam (North-east India): a multifaceted analytical approach. Int. J. Coal Geol. 137:19-37. doi:10.1016/j.coal.2014.11.002.
- Silva, L. F. O., and K. M. da Boit. 2011. Nanominerals and nanoparticles in feed coal and bottom ash: implications for human health effects. Environ. Monit. Assess. 174 (1-4):187-197. doi:10.1007/s10661-010-1449-9.
- Utsunomiya, S., and R. C. Ewing. 2003. Application of high-angle annular dark field scanning transmission electron microscopy, scanning transmission electron microscopy-energy dispersive X-ray spectrometry, and energyfiltered transmission electron microscopy to the characterization of nanoparticles in the environment. Environ. Sci. Technol. 37:786-791. doi:10.1021/es026053t.
- Utsunomiya, S., K. A. Jensen, G. J. Keeler, and R. C. Ewing. 2002. Uraninite and fullerene in atmospheric particulates. Technol. 36:4943-4947. doi:10.1021/ Environ. Sci. es025872a.
- Utsunomiya, S., K. A. Jensen, G. J. Keeler, and R. C. Ewing. 2004. Direct identification of trace metals in fine and ultrafine particles in the Detroit urban atmosphere. Environ. Sci. Technol. 38:2289-2297. doi:10.1021/es035010p.
- Utsunomiya, S., M. Kogawa, E. Kamiishi, and R. C. Ewing. 2011. Scanning transmission electron microscopy and related techniques for research on actinide and radionuclide nanomaterials. In Actinide nanoparticle research, ed. S. N. Kalmykov and M. A. Denecke, 33-62. Springer.
- Vassilev, S. V., and C. G. Vassileva. 2005. Methods for characterization of composition of fly ashes from coal-fired power stations: a critical overview. Energy Fuels 19: 1084-1098. doi:10.1021/ef049694d.
- Wang, Y., X. Li, and J. O. Wendt. 2018. Ash aerosol and deposition formation mechanisms during air/ oxy-combustion of rice husks in a 100 kW combustor. 32:4391-4398. Energy Fuels doi:10.1021/acs.ener gyfuels.7b03127.
- Wang, Y., X. Li, and J. O. L. Wendt. 2019. On ash deposition rates from air and Oxy-Combustion of pulverized coal, petroleum coke, and biomass. Energy Fuels. doi: 10.1021/acs.energyfuels.8b04185.
- Xu, M., D. Yu, H. Yao, X. Liu, and Y. Qiao. 2011. Coal combustion-generated aerosols: Formation and properties. Proc. Combust. Inst. 33 (1):1681-1697. doi:10.1016/ j.proci.2010.09.014.
- Xu, Y., X. Liu, P. Zhang, J. Guo, J. Han, Z. Zhou, and M. Xu. 2016. Role of chlorine in ultrafine particulate matter formation during the combustion of a blend of high-Cl coal and low-Cl coal. Fuel 184:185-191.
- Zhan, Z., L. E. Bool, A. Fry, W. Fan, M. Xu, D. Yu, and J. O. L. Wendt. 2013. Novel temperature-controlled ash deposition probe system and its application to oxy-coal combustion with 50% inlet O2. Energy Fuels 28:146-154. doi:10.1021/ef4014899.
- Zhan, Z., A. Fry, Y. Zhang, and J. O. L. Wendt. 2015. Ash aerosol formation from oxy-coal combustion and its



- relation to ash deposit chemistry. Proc. Combust. Inst. 35 (2):2373–2380. doi:10.1016/j.proci.2014.07.001.
- Zhan, Z., S. Tian, A. Fry, and J. O. L. Wendt. 2016. Formation of ash aerosols and ash deposits of coal blends. In Clean coal technology and sustainable development, ed. G. Yue and S. Li, 121-131. Springer.
- Zhan, Z., and J. O. L. Wendt. 2017. Role of sodium in coal in determining deposition rates. Energy Fuels 31: 2198-2202. doi:10.1021/acs.energyfuels.6b02183.
- Zhang, J., K. E. Kelly, E. G. Eddings, and J. O. L. Wendt. 2011. CO<sub>2</sub> effects on near field aerodynamic phenomena in 40 kW, co-axial, oxy-coal, turbulent diffusion flames. Int. J. Greenhouse Gas Control 5:S47-S57. doi:10.1016/j.ijggc.2011.05.022.
- Zhou, M.-M., J. C. Parra-Álvarez, P. J. Smith, B. J. Isaac, J. N. Thornock, Y. Wang, and S. T. Smith. 2019. Largeeddy simulation of ash deposition in a large-scale laboratory furnace. Proc. Combust. Inst. 37 (4):4409-4418. doi: 10.1016/j.proci.2018.09.034.